

Ultrafast Photochemistry and Electron Diffraction for Cyclobutanone in the S_2 State: Surface Hopping with Time-Dependent Density Functional Theory

Ericka Roy Miller,^{1, a)} Sean J. Hoehn,^{1, a)} Abhijith Kumar,¹ Dehua Jiang,¹ and Shane M. Parker^{1, b)}

*Department of Chemistry, Case Western Reserve University
10900 Euclid Ave, Cleveland, OH 44106, USA*

We simulate the photodynamics of gas-phase cyclobutanone excited to the S_2 state using fewest switches surface hopping (FSSH) dynamics powered by time-dependent density functional theory (TDDFT). We predict a total C3+C2 photoproduct yield of 9%, with a C3:C2 product ratio of 1:8. Two primary $S_2 \rightarrow S_1$ conical intersections are identified: β stretch and CCH bend, with the higher energy β stretch being associated with sub-picosecond S_2 decay. Excited state lifetimes computed with respect to electronic state populations were found to be 7.0 ps ($S_2 \rightarrow S_1$) and 550 fs ($S_1 \rightarrow S_0$). We also generate time-resolved difference pair distribution functions (Δ PDFs) from our TDDFT-FSSH dynamics results in order to generate direct comparisons to ultrafast electron diffraction experiment observables. Global and target analysis of time-resolved Δ PDFs produced a distinct set of lifetimes: i) a 0.462 ps decay, and ii) a 16.8 ps decay that both resemble the S_2 minimum, as well as iii) a long ($>$ nanosecond) decay that resembles the S_1 minimum geometry and the fully separated C3/C2 products. Finally, we contextualize our results by considering the impact of the most likely sources of significant errors.

I. INTRODUCTION

Photochemical processes involve tightly coupled electronic and nuclear motions occurring on ultrafast timescales. Unraveling the detailed mechanisms of these processes has relied on an equally tight synergy between advanced experimental and computational techniques. The most commonly applied experimental techniques with ultrafast time resolution are transient spectroscopy experiments such as transient UV-vis absorption spectroscopy,¹ time-resolved infrared spectroscopy,² or time-resolved X-ray absorption spectroscopy.³ Transient spectroscopies uncover photochemical reactivities by probing the evolution of the electronic or vibronic structure over time. However, these approaches can only provide indirect evidence about chemical structure, such as interatomic distances. Instead, structural information is typically inferred by comparing with simulations. Nonadiabatic molecular dynamics (NAMD) simulations have emerged as a powerful complement to ultrafast experiments for photochemical reactions.⁴⁻⁶ At a conceptual level, NAMD simulations produce molecular movies that show the movement of electrons and nuclei in response to absorbed light. Hence, NAMD simulations can provide the atomic-scale insights unavailable from transient spectroscopies, provided the simulations are accurate analogues of the experiment. One consequence of the lack of direct experimental structural information is that the accuracy of NAMD simulations is difficult to assess without a direct comparison to experiment.

Over the last decade, ultrafast electron diffraction (UED) experiments using megaelectron-volt (MeV) electrons have proven capable of providing time-resolved structural information with femtosecond time resolution and sub-Ångstrom spatial resolution.^{7,8} Recent applications of UED have thus provided some of the first direct measurements of both electronic and nuclear dynamics in photochemical reactions.⁹⁻¹⁴

The time-resolved structural information provided by UED experiments provides the first opportunity to test the structural predictions of NAMD simulations. Indeed, this Special Topics collection was prepared in recognition of this opportunity, and to encourage the further development of accurate NAMD methods. The challenge as presented by the organizers of this Special Topics collection is to simulate the photochemical dynamics of cyclobutanone (CB) after excitation with a 200 nm laser pulse, including the prediction of time-resolved structural measurements. Simultaneously, a set of UED experiments will be performed to serve as a time-limited double-blind test of the NAMD simulations.¹⁵

Cyclobutanone is a valuable synthetic precursor,^{16,17} with a diverse set of photo-dissociation pathways that have been intensively investigated both experimentally and computationally. The primary focus of both experimental and computational studies has been on photochemical pathways present after initial excitation to the weakly absorbing S_1 state. Two categories of photo-products are seen for cyclobutanone: the C3 products, consisting of C_3H_6 and CO, and the C2 products, consisting of C_2H_4 and CH_2CO . The ratio of C3:C2 products has been shown to be wavelength dependent: longer wavelength excitations favor C3 products, while shorter wavelength excitations tend to favor C2 products.¹⁸ There has been much debate as to the mechanisms underlying these product ratios. One hypothesis has been that an $S_1 \rightarrow T_1$ intersystem crossing pathway leading to C3 products is in competition with an $S_1 \rightarrow S_0$ internal conversion process leading to C2 products.¹⁸⁻²¹ However, ab-initio multiple spawning (AIMS) simulations with complete active space self-consistent field (CASSCF) found the existence of 3 distinct $S_1 \rightarrow S_0$ conical intersections, where progression through each produced different C3:C2 product ratios.²¹

Comparatively fewer investigations have focused on the photodynamics upon excitation at 200 nm, which corresponds to excitation of the S_2 state. Time-resolved mass spectrometry experiments have shown a rapid sub-picosecond decay from S_2 to S_1 involving a ring-puckering vibrational mode.²² Supporting simulations have shown biexponential decay from S_2

^{a)}These authors contributed equally to this work

^{b)}Electronic mail: shane.parker@case.edu

to S_1 , involving an ultrafast 0.95 ps decay and a slower 6.32 ps decay.²³

In summary, simulating the photodynamics of CB after excitation with 200 nm light will require balancing competing pathways of internal conversion and intersystem crossing, that end in one of two sets of photoproducts, and that may form intermediates with a diradical ground state.

For this challenge, we have selected fewest switches surface hopping²⁴ (FSSH) dynamics powered by time-dependent density functional theory (TDDFT).²⁵ TDDFT is a “workhorse” of photochemical simulations due to its excellent cost-to-performance ratio. In addition, the growing number of successful applications of TDDFT to photochemical problems seems to indicate that it strikes an ideal balance between static and dynamic correlation, which is crucial for accurate photochemistry.^{26–29} However, TDDFT also has several well known deficiencies. Perhaps most concerning, TDDFT fails to produce true conical intersections between the ground state and the first excited state, instead yielding non-interacting seams with incorrect dimensionality.³⁰ Indeed, TDDFT becomes unstable near degenerate ground states. In addition, TDDFT has systematic biases resulting in the underestimation of triplet state energies^{31,32} and charge-transfer states.³³ Finally, DFT with a restricted Kohn-Sham (KS) determinant typically fails to break bonds homolytically because the closed-shell determinant can not describe an open-shell (or diradical) configuration.³⁴

We take a pragmatic approach to predicting the photochemical reactivity of cyclobutanone. In short, we will perform and analyze photochemistry simulations using TDDFT-FSSH, and then perform a series of sensitivity analyses to estimate the potential impact of the above-mentioned deficiencies. To avoid instabilities surrounding $S_1 \rightarrow S_0$ conical intersections, we apply an energy gap threshold to force hops to the ground state during our TDDFT-FSSH dynamics. Intersystem crossing (ISC) effects are excluded entirely from our simulations due to technical limitations of our selected TDDFT-FSSH implementation. Therefore, we estimate the overall impact on final product quantum yields using a Landau-Zener survey of ISC probabilities throughout our dynamics. And finally, we apply a combination of broken-symmetry and unrestricted TDDFT to estimate the possible errors in photoproduct yields caused by our use of a restricted KS determinant in the ground state.

This manuscript is organized as follows. In section II, we describe the computational methods and implementation details of our simulations. Section III describes the results of our photochemistry simulations. Next, in section IV we contextualize the results of our photochemistry simulations with sensitivity analyses to arrive at final predictions for the photochemistry of CB. Finally, we conclude in section V with a summary of our approach and a discussion of the implications of our results both on the photochemistry of CB as well as on the state of predictive photochemistry.

II. COMPUTATIONAL METHODS

For all dynamics simulations and for most of our analysis, we used the TURBOMOLE program suite, version 7.5.³⁵ In addition, we used ORCA³⁶ version 5.0 for the calculation of spin-orbit couplings³⁷, triplet state energies, and for minimum energy conical intersection optimizations. Further details of each stage of our computational methods are given below.

A. Ground State Dynamics

To sample the equilibrium ensemble and to generate initial conditions for our NAMD simulations, we performed 10 ps ground state molecular dynamics simulations using TURBOMOLE. These simulations used the TPSS density functional³⁸ with the def2-SVPD basis set³⁹ and D3(BJ)^{40,41} dispersion corrections. The resolution-of-the-identity technique was used to accelerate the Coulomb integrals (RIJ),⁴² grid size 3 with quadrature weight derivatives were used for functional integration, and a tight SCF convergence threshold of 10^{-9} Eh (\$\$scfconv 9) was used to improve energy conservation. The trajectory was initiated from the ground-state minimum with initial velocities sampled according to the Boltzmann distribution at 500 K. The dynamics were propagated using TURBOMOLE’s frog module with a 20 a.u. (0.484 fs) time step. With these settings, the total energy drift during ground state dynamics was less than $1.6 \mu\text{Hartree/ps}$ and oscillations of the total energy were about $10 \mu\text{Hartree}$.

B. Electronic State Analyses

Electronic states were characterized by computing excited states at the ground-state equilibrium structure (i.e., the Franck-Condon structure), which was optimized with RIJ/TPSS/def2-SVPD/D3(BJ). To compute excited states, we used Linear Response TDDFT within the Tamm-Dancoff approximation⁴³ with the PBE0 density functional,⁴⁴ and again with the def2-SVPD basis set³⁹ and D3(BJ) dispersion corrections.^{40,41} All calculations using the PBE0 functional used the resolution-of-the-identity technique to accelerate both Coulomb and exchange integrals (RIJK). The size 4 grids with quadrature weight derivatives were again used for functional integrations, with tight SCF (10^{-9} Eh) and excited state (residual norm of 10^{-7}) convergence thresholds.

C. Nonadiabatic Molecular Dynamics (NAMD)

All NAMD simulations used TURBOMOLE’s implementation of Tully’s Fewest Switches Surface Hopping (FSSH).²⁴ The dynamics used the RIJK/PBE0/def2-SVPD/D3(BJ) method as described above to compute all the requisite energies, forces, and couplings. Nonadiabatic coupling matrix elements were computed as the inner product of the derivative coupling vectors and the nuclear velocity. Derivative couplings between the ground-and-excited state are

computed using linear response theory⁴⁵ while derivative couplings between two excited states are computed using quadratic response theory²⁹ within the pseudowavefunction approximation.⁴⁶ In both cases, electron translation factors were incorporated by neglecting terms that violate translational invariance.⁴⁷

Initial conditions were sampled randomly from the ground state MD trajectories above, and were initiated on the S_2 state, which corresponds most closely to excitation with 200 nm light. The dynamics were propagated with the leapfrog Verlet algorithm and a time step of 20 a.u. (0.484 fs) for a total time of about 10 ps. After a surface hop, the momenta were rescaled along the direction of the derivative coupling vector to conserve the total energy. If there was insufficient momentum in the direction of the derivative coupling vector to satisfy energy conservation (“frustrated hop”), then no hop occurred and no further action was taken (i.e., there is no reversal of momentum). To avoid instabilities near degenerate ground states, surface hops to the ground state are forced whenever the first excitation energy to S_1 falls below 0.5 eV.

All statistical uncertainties are presented as 95% confidence intervals that were estimated using bootstrap resampling with 10000 samples, unless stated otherwise.^{48,49}

D. Conical Intersection and Excited State Minima Optimizations

Excited state minima for the S_1 and S_2 excited states were computed using RIJK/PBE0/def2-SVPD/D3(BJ). Using molecular geometries extracted from surface hopping structures found during NAMD simulations, we also performed minimal energy conical intersection (MECI) optimizations with ORCA, using RIJK/PBE0/def2-SVPD/D3(BJ).

E. Ultrafast Electron Diffraction Patterns

Ultrafast electron diffraction (UED) patterns were simulated using structural data from our NAMD simulations and used to estimate effective PDFs. As our goal is to compare these PDFs with the experimentally determined PDFs, we used the same basic strategy as the measurements, in which we first compute a modified scattering intensity, $sM(s)$, that includes weighted contributions from all atom pairs in the molecule, and then use the modified scattering intensity to reconstruct the real space pair distribution function (PDF). The modified scattering intensity was computed within the independent atom model, as

$$sM(s) = s \frac{I_{mol}}{I_{atm}} \quad (1)$$

where s is the magnitude of scattering vector, I_{mol} is the molecular scattering intensity, and I_{atm} is the atomic scattering intensity. Explicit expressions for I_{mol} and I_{atm} are provided in the supplementary information. We used code developed by Thomas J. A. Wolf to generate I_{mol} and I_{atm} scattering intensities directly from XYZ structure files.⁵⁰

The real space PDF was calculated from the modified scattering intensity using a Fourier transform,

$$PDF(R) = \int_0^{s_{max}} sM(s) \sin(sR) e^{-ks^2} ds \quad (2)$$

where $s_{max} = 12 \text{ \AA}^{-1}$ is the experimentally determined maximum amplitude of scattering vector, R is the interatomic distance, and $k = 0.03 \text{ \AA}^2$ is a damping factor chosen to tame experimental noise at larger values of s —which we note also has the effect of broadening the PDF. PDFs and modified scattering intensities for the NAMD simulations were averaged over the swarm of trajectories. The change in modified scattering intensity and PDFs were computed by subtracting the intensities and PDFs at $t = 0$, i.e., $\Delta PDF(R, t) = PDF(R, t) - PDF(R, 0)$ and $\Delta sM(s, t) = sM(s, t) - sM(s, 0)$. Finally, to mimic the 150 fs time resolution of UED experiments, we convolved the calculated ΔPDF with a Gaussian kernel having a full-width-at-half-maximum (FWHM) of 150 fs. Without the convolution, the calculated ΔPDF is dominated by high frequency oscillations that would be invisible to the experiments.

F. Landau-Zener analysis

Within the Landau-Zener model, the probability of a molecule undergoing an $S_n \rightarrow T_m$ transition is given by

$$P_{LZ} = 1 - \exp\left(-\frac{2\pi|V_{nm}^{SOC}|^2}{|\dot{\Omega}_{nm}|\hbar}\right) \quad (3)$$

where $|V_{nm}^{SOC}|$ is the magnitude of the spin-orbit coupling matrix element and $\dot{\Omega}_{nm}$ is the rate of change of the energy gap, $\Omega_{nm} = E_n - E_m$, between the states.⁵¹ The spin-orbit coupling matrix elements were computed using ORCA.^{36,37} The rate of change of the energy gap was computed using a finite difference approximation,

$$\dot{\Omega}_{nm}(t) = \frac{d}{dt} \Omega_{nm}(t) \approx \frac{\Omega_{nm}(t + \Delta t) - \Omega_{nm}(t)}{\Delta t} \quad (4)$$

where t is the time of an individual snapshot of the trajectory and Δt is the time step. Trajectories were sampled evenly at every 200th time step. Spin orbit couplings and energy gaps were computed between the five lowest energy singlet and triplet states at each sampled point.

G. Reaction Path Analysis

Reaction path analysis was performed using TURBOMOLE. Structures were generated using linear synchronous transit interpolation⁵² via the WOELFLING module. Restricted and unrestricted Kohn-Sham singlet ground state energies were computed using RIJK/PBE0/def2-SVPD/D3(BJ). However, the unrestricted Kohn-Sham energies were obtained using unrestricted triplet ground state orbitals as the initial guess prior to final wavefunction optimization.

H. Broken-Symmetry TDDFT

We use the broken-symmetry TDDFT (BRS-TDDFT) approach as implemented in TURBOMOLE and reported previously.^{27,34} In brief, at each time step a triplet instability calculation is used to check whether a lower energy unrestricted Kohn-Sham determinant is available. If such a state is found, the spin symmetry is broken and the simulation is continued. Besides this modification, the remainder of the NAMD simulation is identical to the one described above.

III. PHOTOCHEMISTRY SIMULATIONS

In this section, we present the results of our PBE0-FSSH simulation of cyclobutanone. We give a brief overview of the structural and electronic features of cyclobutanone at its Franck-Condon geometry. We then derive conclusions about excited state decay lifetimes and pathways directly from our simulated data, before rendering our dynamics results in terms of UED observables.

A. The Franck-Condon Regime of Cyclobutanone

The PDF of the S_0 equilibrium structure of cyclobutanone is shown in Figure 1. Primary contributions to the first peak include the CO bond and the CC bonds. At the Franck-Condon geometry there is near perfect overlap between the bond length between carbonyl and α -carbons and the bond length between α -carbons and β -carbons. Going forward, these bonds will be referred to as α -CC and β -CC bonds respectively. The second peak is composed primarily of signals from non-bonding and cross-ring diagonals, with an extended shoulder originating from non-bonding CH and OH interactions.

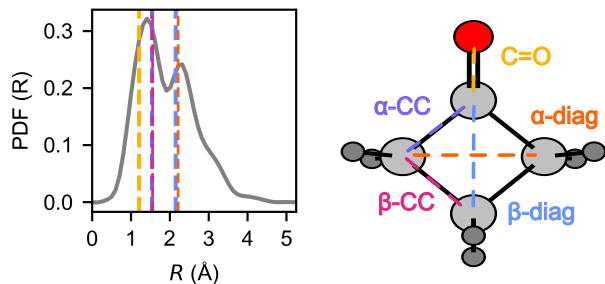


FIG. 1. Simulated PDF for optimized S_0 minimum geometry of cyclobutanone.

Using PBE0, we characterized the first three singlet states of cyclobutanone. The results are collected in Table I. As shown in Table I, qualitative agreement was found between the simulated excitation energies and the spectroscopically bright state targeted by the 200 nm (6.2 eV) laser probe. We find that PBE0 overestimates the excitation energies relative

to the experimental values. More specifically, the S_1 excitation computed using PBE0 is 4.22 eV, compared to the experimental value of 3.92 eV. Similarly, the S_2 state computed using PBE0 is 6.83 eV, compared to the experimental value of 6.36 eV. Nonetheless, we unambiguously identify that the S_2 state is most likely to be excited at 200 nm, both because it is closest in energy and because it is brightest. Thus, we performed PBE0-FSSH simulations starting from the S_2 state using a swarm of 100 trajectories. In the following, we present the results of these simulations.

TABLE I. Computational and experimental characterization of the three lowest energy singlet states of cyclobutanone

State	VEE ^a (eV)	f^b	Absorption Peak (eV)	f^c	Transition
S_1	4.22	6.9×10^{-6}	3.92 ^d	5×10^{-4}	$n \rightarrow \pi^*$
S_2	6.83	4.0×10^{-2}	6.36 ^e	3×10^{-2}	$n \rightarrow 3s$
S_3	7.44	1.8×10^{-5}	7.08 ^f	7×10^{-3}	$n \rightarrow 3p$

^a vertical excitation energies using RIJK/PBE0/def2-SVPD/D3(BJ) from S_0 minimum structure

^b length representation oscillator strengths

^c estimated oscillator strengths by Whitlock and Duncan⁵³

^d gas phase absorption band maximum⁵⁴

^e gas phase absorption band maximum⁵⁵

^f gas phase absorption band maximum⁵⁵

B. Excited-state dynamics and lifetimes

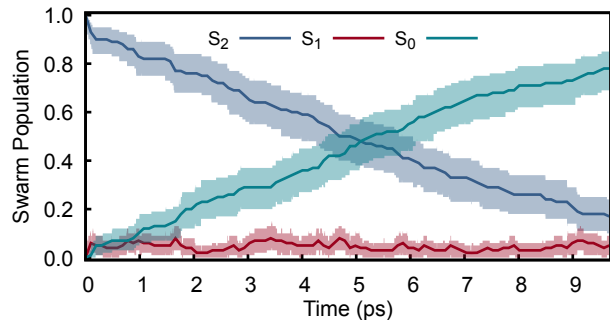


FIG. 2. Excited state populations measured over trajectory swarms. Shaded regions show the 95% bootstrap confidence interval.

The qualitative behavior of most of the trajectories followed a similar pattern. After excitation to the S_2 state, CB undergoes quick decay to the S_1 state, followed by even faster decay to the S_0 state. Figure 2 shows the excited state populations as a function of time for the swarm of trajectories over the 10 ps simulation time. Here, we see a steady decay of the S_2 population, ending with an S_2 population of 17%. We determine a time constant for the decay by first determining the half-life (i.e., the time at which $P_2(t) = 1/2$), and then assuming a single exponential decay for the S_2 swarm population, $P_2(t) = \exp(-t/\tau_2)$. We find a half-life of 4.9 ps (CI: 4.2–6.2

ps) which corresponds to a time constant of $\tau_2 = 7.0$ ps (CI: 6.1–8.9 ps).

The S_1 population, by contrast, has an essentially steady-state behavior, oscillating around 5% for most of the simulation time. This indicates that the S_1 state is much shorter lived than the S_2 state. We estimate the S_1 lifetime by computing the average residence time spent in the S_1 state as $\bar{t}_1 = t_{1 \rightarrow 0} - t_{2 \rightarrow 1}$ where $t_{1 \rightarrow 0}$ and $t_{2 \rightarrow 1}$ are the times at which the $S_1 \rightarrow S_0$ and $S_2 \rightarrow S_1$ hops occur, respectively, limiting this analysis to the 77 trajectories that underwent this pathway. We find a mean residence time of $\bar{t}_1 = 550$ fs (CI: 460–650 fs). If we assume that, once generated, the S_1 state decays exponentially as $P_1(t') = \exp(-t'/\tau_1)$, where t' is the time since the S_1 state was first populated, then the mean residence time is also the lifetime, i.e., $\tau_1 = \bar{t}_1$.

C. Decay Pathways and Conical Intersections

Figure 3 shows the distribution of hopping structures observed during PBE0-FSSH dynamics. We observe two distinct modes for $S_2 \rightarrow S_1$ deactivation, which we characterize as either a β stretch, where one of the β -CC bonds stretches from an equilibrium value of about 1.6 Å to the range of 2.0–2.2 Å, or a CCH bend, in which one of the CCH angles formed between an α -CC bond and a CH bond decreases from an equilibrium value of about 110° to the range of 90–100°. MECI optimizations starting from these hopping structures identified two dominant $S_2 \rightarrow S_1$ structures, representatives for which are shown in Figure 4. The β stretch MECI structure representative has a β -CC bond length of 2.1 Å, while the representative CCH bend MECI structure has a CCH angle of 71°. Furthermore, we found that 80% of the $S_2 \rightarrow S_1$ deactivations proceeded through the CCH bend structure, 18% proceeded through the β stretch structure, and 2% proceeded through other structures. Interestingly, although the majority of $S_2 \rightarrow S_1$ deactivations occurred through the CCH bend structure, those that decayed through the β stretch structure were significantly more reactive. 11 out of the 15 trajectories that decayed via β stretch did so within the first picosecond after photoexcitation, compared to only 5 out of 66 trajectories that deactivated through a CCH bend structure. Considering only the 15 trajectories that decayed via β stretch, the mean residence time in the S_2 state was 0.8 ps, in partial agreement with the fast decay component of 0.95 ps found by Kuhlman et al.²³ Notably, the representative β stretch structure displayed in Figure 4 is around 0.8 eV higher in energy than the representative CCH bend structure.

Comparatively less distinction was found in $S_1 \rightarrow S_0$ hopping structures. The only significant coordinate we observed was the α -CC stretch, which were found to be broadly distributed from 1.6 Å to 2.5 Å, compared to an equilibrium value of 1.5 Å. MECI optimizations confirmed only one dominant $S_1 \rightarrow S_0$ structure, denoted in Figure 4 as α stretch.

Figure 4 shows an overview of the observed decay pathways, including C3/C2 product formation. Out of the 100 PBE0-FSSH trajectories, only 9% resulted in photodissociation products within 10 ps, with a C3:C2 product ratio of 1:8.

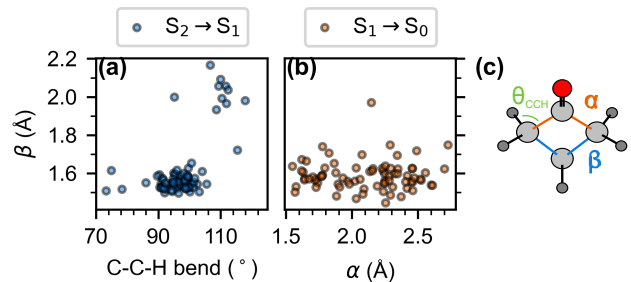


FIG. 3. Structural characterization of hopping structures observed in the NAMD simulations for (a) $S_2 \rightarrow S_1$ hops and (b) $S_1 \rightarrow S_0$ hops.

A detailed breakdown of trajectory outcomes can be found in Tables SI and SII.

D. Ultrafast Electron Diffraction (UED) Simulations

As a direct comparison to experimental observables, we computed time-resolved Δ PDFs by averaging across all 100 trajectories in the NAMD swarm. The results are shown in Figure 5. In addition, more detailed views of specific time windows are shown in Figure 6.

As shown in Figure 5 and Figure 6a, immediately following UV excitation, positive amplitude in Δ PDF were observed at distances of ca. 1, 1.9, 2.7, and 3.7 Å. Simultaneously, within the first approximate 0.5 ps after excitation, negative Δ PDF bands were observed to grow in magnitude at ca. 1.5 and 3.1 Å. Between ca. 0.5 ps and 3.5 ps (Figure 6b), the bands at ca. 1, 1.9, and 2.7 Å decrease in intensity, with a new band growing negatively in amplitude at ca. 2.3 Å. Interestingly, a slight increase in intensity is observed at ca. 3.7 Å, while the two negative signals at ca. 1.5 and 3.1 Å remain unchanged.

Lastly, from ca. 3.5 ps to 9.6 ps as shown in Figure 6c, the bands at ca. 1, 2.3, and 2.7 Å continue to grow negatively in magnitude, with the band at ca. 1 Å shifting to shorter distances and broadening simultaneously. The remaining bands on the simulated distributions appear to have minimal changes in amplitude.

In order to contextualize these time-resolved Δ PDFs band structures, we compare normalized Δ PDFs of relevant structures and extracted evolution associated decay distributions (EADD) in Figure 7. EADD were obtained from applying global and target analyses⁵⁶ to the simulated data using a two-component with an offset, sequential kinetic model via the Glotaran graphical user interface to the R-package TIMP software.⁵⁷ The EADD are direct analogies of evolution associated decay spectra commonly used to analyze transient spectra, but we emphasize here that these are pair distributions, *not spectra*. Lifetimes from this analysis using an instrument response function (IRF) of 60 fs, were 0.462 ± 0.004 ps and 16.8 ± 0.3 ps. This finding of a short sub-picosecond lifetime and a longer picosecond lifetime is consistent with our observation of two distinct decay modes out of the S_2 state, with the shorter lifetime of about 0.8 ps. In addition, a long time offset

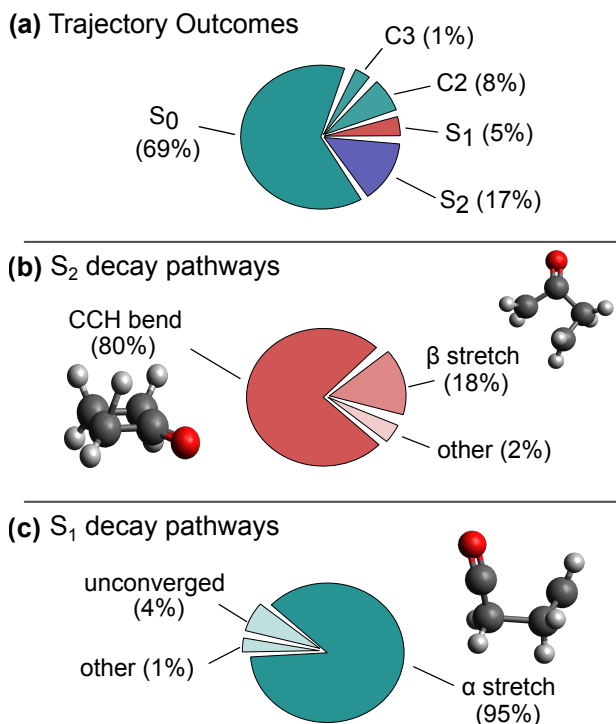


FIG. 4. **(a)** Breakdown of PBE0-FSSH dynamics outcomes. S₂ and S₁ categories refer to trajectories that remained in these respective excited states, while C2, C3, and S₀ categories reflect product ratios of trajectories that decayed to the S₀ state, optionally undergoing photodissociation. Percentages are given with respect to the 100 trajectories that completed the full 10 ps simulation time. **(b)** Breakdown of pathways of S₂ decay pathways. Representative structures of the β stretch and CCH bend S₂→S₁ conical intersections are shown. Percentages are given with respect to the 83 trajectories that decayed from the S₂ state. **(c)** Breakdown of pathways for S₁ decay pathways. A representative structure of the α stretch S₁→S₀ conical intersection is shown. Percentages are given with respect to the 76 trajectories that decayed from the S₁ state.

was found with greater than nanosecond lifetime. Errors are reported as twice the standard deviation. We note that the lifetimes computed here, reflecting only structural information, differ significantly from the earlier lifetimes computed from electronic state information. This difference strongly emphasizes the need to use the same observables when comparing simulated and measured results, as there is no strong *a priori* reason why the timescales from two different observables must agree.

As shown in Figure 7a, EADD1 and EADD2, which correspond to the 0.462 ps and 16.8 ps lifetimes, line up well with the Δ PDF of the S₂ minimum. From EADD3 (Figure 7b), these signals were found to overlap well with Δ PDF for the S₁ and fully separated C3/C2 products.

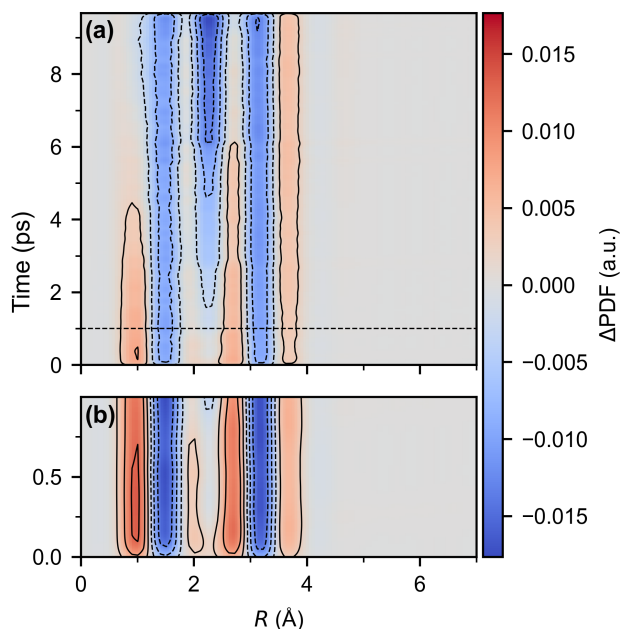


FIG. 5. Contour plot of Δ PDF averaged across all 100 trajectories for **(a)** the full simulated time regime of 0 - ca. 10 ps, and **(b)** the ultrafast 0-1 ps regime. The horizontal line in **(a)** shows the time window in **(b)**.

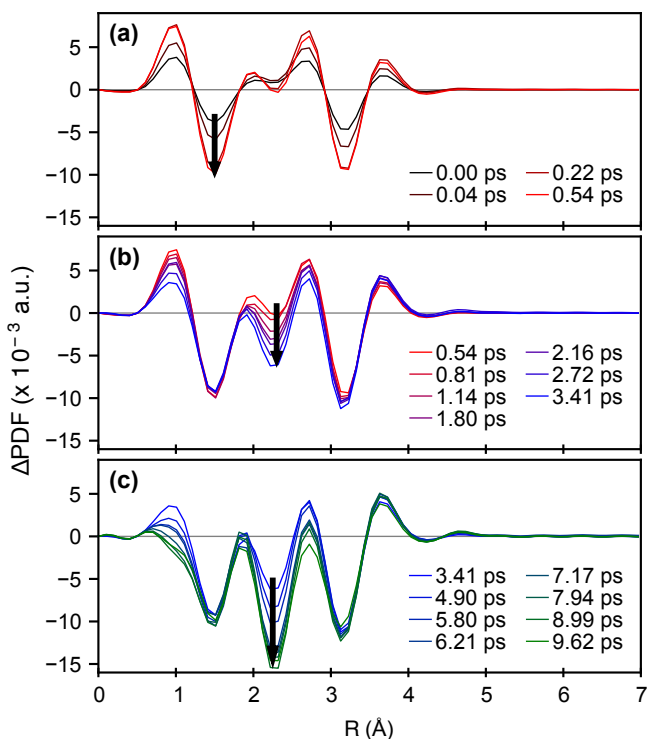


FIG. 6. Simulated Δ PDF at select time delays after photo-excitation from a) 0-0.5 ps, b) 0.5-1.8 ps and c) 3.4-9.6 ps.

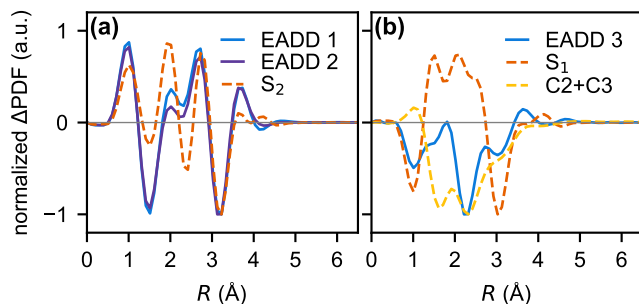


FIG. 7. Comparison of extracted EADS from global and target analyses of the simulated time-resolved Δ PDF with normalized Δ PDF of critical structures. (a) EADD1 and EADD2 compared to the Δ PDF for the S_2 minimum. (b) EADD3 compared to the Δ PDF for the S_1 minimum and the C3 and C2 products.

IV. SENSITIVITY ANALYSES OF PHOTOCHEMISTRY SIMULATIONS

Due to technical limitations, our simulations used a closed shell reference and only included singlet excited states. Therefore, in this section, we attempt to put the PBE0-FSSH simulations in greater context by performing sensitivity analyses of our most likely sources of error: intersystem crossing and ground state diradical formation.

A. How likely is intersystem crossing?

Here, we attempt to quantify the impact of omitting ISC effects by estimating the probability of ISC using a Landau-Zener-based approach. Landau-Zener estimates transition probabilities between two diabatic states under the assumption that i) the states cross in energy, ii) the energy gap between them changes linearly with time, and iii) the diabatic coupling between the two states is constant. In this framework, ISC is enhanced when the energy gap changes slowly and the diabatic coupling is large.

We estimated the probability of ISC in cyclobutanone by extracting energy gap rates and spin-orbit coupling matrix elements from a subset of 9 PBE0-FSSH trajectories at an interval of 0.1 ps. From these snapshots, we determined the root-mean-square (RMS) and standard deviation of the energy gap rates and spin-orbit coupling matrix elements (see Tables SIII - V of the supplementary information). Finally, we used these to estimate confidence intervals for the probability of ISC. The results are shown in Figure 8. From here we see that the probability of ISC is low for all estimates. For example, using the RMS values, we find the ISC probability to be less than 0.5% in all cases. Estimating the ISC probability using energy gap rates that are one standard deviation lower than the RMS and spin-orbit couplings that are one standard deviation larger than the RMS, we still find an ISC probability of less than 3% in all cases. We emphasize that these are estimating the probability of an ISC event *each time two states cross in energy*. The actual ISC probabilities may be

lower because not all states cross. Therefore, we conclude that the overall yield of ISC is likely to be less than 10-20% in cyclobutanone, and thus our simulations describe at least 80-90% of the photoproduct channels. We note that this contrasts sharply with the near 100% yield of ISC observed in the gas phase photochemistry of cyclobutanone when excited using 300-320 nm light.^{19,20} We speculate that this discrepancy is due to the higher photon energy used here, which leads to more nuclear kinetic energy during the photochemical reaction and thus lower ISC yields within the Landau-Zener picture. Such a phenomenon has been observed in other photochemical reactions. For example, the relative rate of internal conversion in hexafluoroacetone has been found to increase with increasing photon energy.⁵⁸

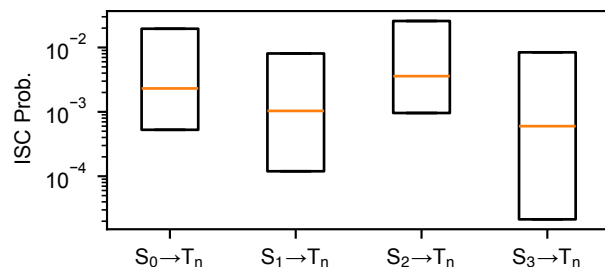


FIG. 8. Confidence intervals for the probability of intersystem crossing (ISC) in cyclobutanone. The orange line shows the ISC probability using root mean square (RMS) values for energy gap rates and spin-orbit couplings. The box shows the range of ISC probabilities using energy gap rates and spin-orbit couplings that are one standard deviation away from the RMS. Maximum values for ISC probabilities for each singlet state to the triplet manifold are displayed.

B. Is the ground state ever a diradical?

We observed from our simulations that the overall photoproduct yield of about 9% within the first 10 ps of the simulation was lower than expected based on prior experimental results. For example, photoproduct yields of 10-22% are observed in the liquid phase and estimated to be 30-40% in the gas phase when exciting in the 300 nm to 320 nm wavelength window.^{19,20} Our naive expectation was that the higher photon energy used here would in turn lead to larger photoproduct yields. Moreover, prior experimental results found nearly equal C3:C2 ratios, ranging from about C3:C2 of 1:2 to 2:1,¹⁹ whereas our results indicate a C3:C2 ratio of 1:8. Thus, we test whether our methodology was systematically underestimating the yield of photoproducts in general, and the C3 products in particular.

The likely culprit for an anomalously low photoproduct yield would be use of a restricted Kohn-Sham (RKS) reference for the ground state. Consequently, diradical or open-shell ground states are not accessible. Open-shell singlet excited states, on the other hand, are correctly described within TDDFT as singlet excitations out of the closed-shell reference. Although all the photoproducts of cyclobutanone are

expected to be closed-shell, we considered the possibility that there could be reaction intermediates with diradical character. To test this, we performed a series of broken-symmetry TDDFT simulations to determine whether the ground state of cyclobutanone becomes diradical.

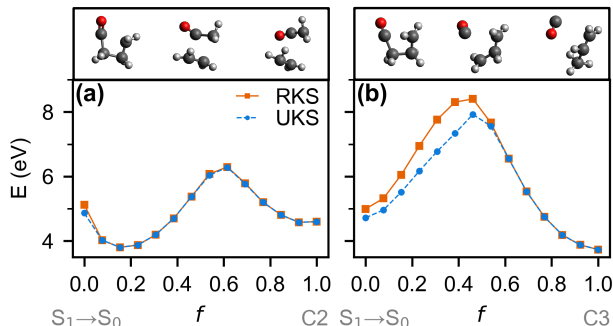


FIG. 9. Comparison of RKS and UKS energies along representative dissociation paths leading to a) C2 and b) C3 photoproducts. The reaction path was generated by interpolating between a representative hopping structure ($f = 0$) and dissociated products ($f = 1$) using the linear synchronous transit method.⁵² Energies are relative to the S_0 minimum. Above each plot are the starting, highest energy intermediate, and ending structures of the reaction path.

First, we wanted to determine whether diradical intermediates might be important for the formation of photoproducts *during the dynamical simulations*. To test this, we scanned the potential energy connecting representative $S_1 \rightarrow S_0$ hopping structures to either the C2 or C3 photoproducts. We used the linear synchronous transit⁵² method to interpolate between hopping structures and photoproducts and then computed ground state energies using both restricted (RKS) and unrestricted Kohn-Sham (UKS) calculations. We use the highest energy found for each interpolated path as a rough approximation for the reaction barrier, although we note that they are in fact upper bounds. As shown in Figure 9, we found no differences between the C2 product reaction barrier computed using RKS and UKS. On the other hand, broken symmetry solutions were indeed found along the C3 reaction path. The approximate barrier height along the C3 path was lower by about 0.5 eV using UKS than was found with RKS. However, we argue here that this is a *quantitative* rather than *qualitative* error, because using a UKS reference changes the barrier heights but not the overall shape of the reaction path. Thus, we conclude that RKS likely underestimates the yield of C3 photoproducts, but that the qualitative behavior of photoproduct formation is likely consistent between RKS and UKS.

Next, we wanted to determine whether the photon energy by itself was sufficient to form photoproducts, and whether a diradical ground state was essential to that reactivity. To do this, we performed a series of 5 ps BRS-TDDFT simulations with initial nuclear velocities sampled from a temperature of 2716 K, 4363 K, and 10000K, which give total kinetic energies equivalent to the energy of a 387 nm (3.2 eV), 243 nm (5.1 eV) photon, and 87 nm (14.3eV) respectively. This is equivalent to assuming the photon energy is immediately

converted into thermal energy, and thus we consider the products formed in this case as thermal products. For the simulations at 2716 K (3.2 eV) and 4363 K (5.1 eV), we saw no evidence of thermal product formation and no evidence of a diradical ground state. With an initial temperature of 10000 K (14.3eV), the molecule quickly dissociated, leading to convergence failures for the BRS-TDDFT calculations. These results are at least consistent with our findings from the reaction path analysis, as the energy difference between the highest energy intermediate and the optimized ground state minimum is 6.3 eV for C2 dissociation and 7.9 eV for C3 dissociation using UKS. Thus, we conclude that thermal energy of 5.1 eV is not sufficient to form products on a 5 ps timescale.

V. CONCLUSION

The ultrafast photochemistry of cyclobutanone is rich and complex, and thus an excellent target for a double-blind benchmark of modern simulation and experimental techniques. In this work, we took a pragmatic “workhorse” approach to simulating the photochemistry of cyclobutanone, using TDDFT-based surface hopping to simulate the excited state dynamics and ultrafast electron diffraction (UED) patterns. Our simulations indicate that when excited using 200 nm light, cyclobutanone photoexcites into the S_2 state, which then decays sequentially from $S_2 \rightarrow S_1$ with a time constant of about 7.0 ps, and then from $S_1 \rightarrow S_0$ with a time constant of about 550 fs. However, the picture is slightly different when considering the ultrafast electron diffraction patterns. A global and targeted analysis of the time-resolved Δ PDF indicate two important time scales after the initial rise of the excited state: i) a 0.462 ps decay with an associated UED pattern that closely resembles the Δ PDF of the S_2 minimum geometry, and ii) a longer 16.8 ps decay that resembles a combination of the S_1 minimum geometry and the fully separated C3/C2 products. The difference between the timescales obtained from the electronic states and the analysis of the time-resolved UED underscores the need for direct comparisons between experimental and computational observables.

To complement our photodynamics simulations, we performed a series of sensitivity analyses to estimate the magnitude of the most likely sources of error. We consider this analysis to be part of a “pre-mortem” of our results, and we use them to answer the question “If our results end up with significant qualitative failures, what are the most likely sources of error?” In our estimation, the most likely reasons for qualitative failure are the neglect of intersystem crossing (ISC) and underestimation of the C3 photoproduct yields. The restriction to singlet states in our simulations is a technical limitation of the current implementation which will be addressed in future work. We estimated overall triplet yields to be less than 10-20% in cyclobutanone, but the high degree of uncertainty in this estimate limits our confidence.

We expect our simulations to underestimate the overall photoproduct yield for two reasons. First, the inability of TDDFT to recover true conical intersections between the ground state and the first excited state can overestimate in-

ternal conversion pathways and thus miss some relevant photodecay pathways.⁵⁹ Second, we found evidence that the dissociation pathway leading to C3 photoproducts likely involves a diradical ground state, which is not captured with our restricted Kohn-Sham reference. Thus, we expect that the overall photoproduct yield is likely higher than the 9% we observed, and that the C3:C2 ratio is likely closer to 1:1 than the 1:8 we observed. In addition, even if the overall yield is approximately correct, the low number of reactive trajectories would lead to high uncertainty in the C3:C2 ratio. More systematic approaches to simulating surface hopping swarms would be needed to determine the C3:C2 ratio with higher confidence.⁶⁰

Of course, an additional potential outcome is that the reason for any discrepancy between our simulations and the experimental results is completely unforeseen. Regardless of the outcome of the prediction challenge, we believe this combination of prediction and uncertainty estimation will be a valuable approach for photochemistry simulation, where the reactivities are especially complex.

SUPPLEMENTARY MATERIAL

The supplementary material contains detailed statistics for each of our PBE0-FSSH trajectories, details of the implementation of our simulated electron diffraction patterns, along with $sM(s)$ and $\Delta sM(s)$ plots for selected structures, and extended data from our Landau-Zener analysis.

ACKNOWLEDGMENTS

The authors thank Erqian Mao for partaking in discussions in the planning stages of this manuscript. This work was supported by a startup fund from Case Western Reserve University. This work made use of the High Performance Computing Resource in the Core Facility for Advanced Research Computing at Case Western Reserve University.

DATA AVAILABILITY

The code and data that support the findings of this study are openly available in “Ultrafast Photochemistry and Electron Diffraction for Cyclobutanone in the S2 State” at <https://osf.io/m8sbq>.

AUTHOR CONTRIBUTIONS

Ericksa Roy Miller: project administration (lead); conceptualization (equal); methodology (equal) investigation (supporting); visualization (equal); writing - original draft (lead); writing - review and editing (equal). **Sean J. Hoehn:** conceptualization (equal); methodology (equal); investigation (lead);

visualization (equal); writing - original draft (equal); writing - review and editing (equal). **Abhijith Kumar:** conceptualization (equal); methodology (supporting); investigation (supporting); visualization (supporting); writing - original draft (supporting); writing - review and editing (supporting). **Dehua Jiang:** conceptualization (equal); methodology (supporting); investigation (supporting); visualization (supporting); writing - original draft (supporting); writing - review and editing (supporting). **Shane M. Parker:** supervision (lead); conceptualization (equal); methodology (equal); visualization (equal); writing - original draft (equal); writing - review and editing (lead).

- ¹R. Berera, R. van Grondelle, and J. T. M. Kennis, *Photosynth. Res.* **101**, 105 (2009).
- ²A. Mezzetti and W. Leibl, *Photosynth. Res.* **131**, 121 (2017).
- ³R. Geneaux, H. J. B. Marroux, A. Guggenmos, D. M. Neumark, and S. R. Leone, *Philos. Trans. R. Soc., A* **377**, 20170463 (2019).
- ⁴E. Tapavicza, G. D. Bellchambers, J. C. Vincent, and F. Furche, *Phys. Chem. Chem. Phys.* **15**, 18336 (2013).
- ⁵B. F. E. Curchod and T. J. Martínez, *Chem. Rev.* **118**, 3305 (2018).
- ⁶T. R. Nelson, A. J. White, J. A. Bjorgaard, A. E. Sifain, Y. Zhang, B. Negen, S. Fernandez-Alberti, D. Mozyrsky, A. E. Roitberg, and S. Tretiak, *Chem. Rev.* **120**, 2215 (2020).
- ⁷J. Yang, M. Guehr, T. Vecchione, M. S. Robinson, R. Li, N. Hartmann, X. Shen, R. Coffee, J. Corbett, A. Fry, *et al.*, *Nat. Commun.* **7**, 11232 (2016).
- ⁸X. Shen, J. Nunes, J. Yang, R. Jobe, R. Li, M.-F. Lin, B. Moore, M. Niebuhr, S. Weathersby, T. Wolf, *et al.*, *Struct. Dyn.* **6** (2019).
- ⁹J. Yang, X. Zhu, T. J. Wolf, Z. Li, J. P. F. Nunes, R. Coffee, J. P. Cryan, M. Gühr, K. Hegazy, T. F. Heinz, *et al.*, *Science* **361**, 64 (2018).
- ¹⁰Y. Liu, S. L. Horton, J. Yang, J. P. F. Nunes, X. Shen, T. J. Wolf, R. Forbes, C. Cheng, B. Moore, M. Centurion, *et al.*, *Phys. Rev. X* **10**, 021016 (2020).
- ¹¹J. Yang, X. Zhu, J. P. F. Nunes, J. K. Yu, and R. M. Parrish, *Science* **368**, 885 (2020).
- ¹²M. Centurion, T. J. Wolf, and J. Yang, *Annu. Rev. Phys. Chem.* **73**, 21 (2022).
- ¹³D. Filippetto, P. Musumeci, R. Li, B. J. Siwick, M. Otto, M. Centurion, and J. Nunes, *Rev. Mod. Phys.* **94**, 045004 (2022).
- ¹⁴E. G. Champenois, N. H. List, M. Ware, M. Britton, P. H. Bucksbaum, X. Cheng, M. Centurion, J. P. Cryan, R. Forbes, I. Gabalski, *et al.*, *Phys. Rev. Lett.* **131**, 143001 (2023).
- ¹⁵S. Weathersby, G. Brown, M. Centurion, T. Chase, R. Coffee, J. Corbett, J. Eichner, J. Frisch, A. Fry, M. Gühr, *et al.*, *Rev. Sci. Instrum.* **86** (2015).
- ¹⁶K. Tanino, M. Takahashi, Y. Tomata, H. Tokura, T. Uehara, T. Narabu, and M. Miyashita, *Nature Chemistry* **3**, 484 (2011).
- ¹⁷K. Hong, Y. Zhou, H. Yuan, Z. Zhang, J. Huang, S. Dong, W. Hu, Z.-X. Yu, and X. Xu, *Nat. Commun.* **14**, 6378 (2023).
- ¹⁸K. Y. Tang and E. K. C. Lee, *J. Phys. Chem.* **80**, 1833 (1976).
- ¹⁹E. K. Lee, J. C. Hemminger, and C. F. Rusbult, *J. Am. Chem. Soc.* **93**, 1867 (1971).
- ²⁰E. K. Lee, R. G. Shortridge Jr, and C. F. Rusbult, *J. Am. Chem. Soc.* **93**, 1863 (1971).
- ²¹L. Liu and W.-H. Fang, *J. Chem. Phys.* **144** (2016).
- ²²T. S. Kuhlman, T. I. Sølling, and K. B. Møller, *ChemPhysChem* **13**, 820 (2012).
- ²³T. S. Kuhlman, S. Sauer, T. I. Sølling, and K. B. Møller, *J. Chem. Phys.* **137** (2012).
- ²⁴J. C. Tully, *J. Chem. Phys.* **93**, 1061 (1990).
- ²⁵E. Runge and E. K. U. Gross, *Physical Review Letters* **52**, 997 (1984).
- ²⁶E. Tapavicza, I. Tavernelli, and U. Rothlisberger, *Phys. Rev. Lett.* **98**, 023001 (2007).
- ²⁷M. Muuronen, S. M. Parker, E. Berardo, A. Le, M. A. Zwijnenburg, and F. Furche, *Chem. Sci.* **8**, 2179 (2017).
- ²⁸L. Yue, Y. Liu, and C. Zhu, *Phys. Chem. Chem. Phys.* **20**, 24123 (2018).
- ²⁹S. M. Parker, S. Roy, and F. Furche, *Phys. Chem. Chem. Phys.* **21**, 18999 (2019).

- ³⁰B. G. Levine, C. Ko, J. Quenneville, and T. J. Martínez, *Mol. Phys.* **104**, 1039 (2006).
- ³¹D. Jacquemin, E. A. Perpète, I. Ciofini, and C. Adamo, *J. Chem. Theory Comput.* **6**, 1532 (2010).
- ³²M. Casanova-Páez and L. Goerigk, *J. Chem. Phys.* **153**, 064106 (2020).
- ³³A. Dreuw, J. L. Weisman, and M. Head-Gordon, *J. Chem. Phys.* **119**, 2943 (2003).
- ³⁴J. C. Vincent, M. Muuronen, K. C. Pearce, L. N. Mohanam, E. Tapavicza, and F. Furche, *J. Phys. Chem. Lett.* **7**, 4185 (2016).
- ³⁵S. G. Balasubramani, G. P. Chen, S. Coriani, M. Diedenhofen, M. S. Frank, Y. J. Franzke, F. Furche, R. Grotjahn, M. E. Harding, C. Hättig, A. Hellweg, B. Helmich-Paris, C. Holzer, U. Huniar, M. Kaupp, A. Marefat Khah, S. Karbalaei Khani, T. Müller, F. Mack, B. D. Nguyen, S. M. Parker, E. Perlt, D. Rappoport, K. Reiter, S. Roy, M. Rückert, G. Schmitz, M. Sierka, E. Tapavicza, D. P. Tew, C. van Wüllen, V. K. Voora, F. Weigend, A. Wodyński, and J. M. Yu, *J. Chem. Phys.* **152**, 184107 (2020).
- ³⁶F. Neese, F. Wennmohs, U. Becker, and C. Riplinger, *J. Chem. Phys.* **ESS2020**, 224108 (2020).
- ³⁷B. de Souza, G. Farias, F. Neese, and R. Izsák, *J. Chem. Theory Comput.* **15**, 1896 (2019).
- ³⁸J. Tao, J. P. Perdew, V. N. Staroverov, and G. E. Scuseria, *Phys. Rev. Lett.* **91**, 146401 (2003).
- ³⁹D. Rappoport and F. Furche, *J. Chem. Phys.* **133**, 134105 (2010).
- ⁴⁰S. Grimme, J. Antony, S. Ehrlich, and H. Krieg, *J. Chem. Phys.* **132**, 154104 (2010).
- ⁴¹S. Grimme, S. Ehrlich, and L. Goerigk, *Journal of Computational Chemistry* **32**, 1456 (2011).
- ⁴²B. I. Dunlap, J. W. D. Connolly, and J. R. Sabin, *J. Chem. Phys.* **71**, 3396 (1979).
- ⁴³S. Hirata and M. Head-Gordon, *Chem. Phys. Lett.* **314**, 291 (1999).
- ⁴⁴C. Adamo and V. Barone, *J. Chem. Phys.* **110**, 6158 (1999).
- ⁴⁵R. Send and F. Furche, *J. Chem. Phys.* **132**, 044107 (2010).
- ⁴⁶Q. Ou, G. D. Bellchambers, F. Furche, and J. E. Subotnik, *J. Chem. Phys.* **142**, 064114 (2015).
- ⁴⁷S. Fatehi, E. Alguire, Y. Shao, and J. E. Subotnik, *J. Chem. Phys.* **135**, 234105 (2011).
- ⁴⁸B. Efron, *The Annals of Statistics* **7**, 1 (1979).
- ⁴⁹S. Nangia, A. W. Jasper, T. F. Miller, and D. G. Truhlar, *J. Chem. Phys.* **120**, 3586 (2004).
- ⁵⁰T. J. A. Wolf, “Diffraction simulation,” https://github.com/ThomasJAWolf/Diffraction_simulation (2020).
- ⁵¹C. Wittig, *J. Phys. Chem. B* **109**, 8428 (2005).
- ⁵²T. A. Halgren and W. N. Lipscomb, *Chem. Phys. Lett.* **49**, 225 (1977).
- ⁵³R. F. Whitlock and A. B. F. Duncan, *J. Chem. Phys.* **55**, 218 (1971).
- ⁵⁴J. C. Hemminger and E. K. C. Lee, *J. Chem. Phys.* **56**, 5284 (1972).
- ⁵⁵A. Udvarhazi and M. A. El-Sayed, *J. Chem. Phys.* **42**, 3335 (1965).
- ⁵⁶I. H. van Stokkum, D. S. Larsen, and R. van Grondelle, *Biochimica et Biophysica Acta (BBA) - Bioenergetics* **1657**, 82 (2004).
- ⁵⁷J. J. Snellenburg, S. Liptonok, R. Seger, K. M. Mullen, and I. H. M. van Stokkum, *Journal of Statistical Software* **49**, 1–22 (2012).
- ⁵⁸D. A. Knecht, *Chem. Phys. Lett.* **33**, 325 (1975).
- ⁵⁹T. V. Papineau, D. Jacquemin, and M. Vacher, *J. Phys. Chem. Lett.* **15**, 636 (2024).
- ⁶⁰S. M. Parker and C. J. Schiltz, *J. Chem. Phys.* **153**, 174109 (2020).